

See discussions, stats, and author profiles for this publication at: <https://www.researchgate.net/publication/281137768>

# In Situ Mass Spectrometric Determination of Molecular Structural Evolution at the Solid Electrolyte Interphase in Lithium-Ion Batteries

ARTICLE *in* NANO LETTERS · AUGUST 2015

Impact Factor: 13.59 · DOI: 10.1021/acs.nanolett.5b02479 · Source: PubMed

---

READS

51

## 10 AUTHORS, INCLUDING:



Pengfei Yan

Battelle Memorial Institute

27 PUBLICATIONS 89 CITATIONS

[SEE PROFILE](#)



Wu Xu

Pacific Northwest National Laboratory

129 PUBLICATIONS 5,858 CITATIONS

[SEE PROFILE](#)



Rui Zhao

Pacific Northwest National Laboratory

71 PUBLICATIONS 3,248 CITATIONS

[SEE PROFILE](#)



Donald R Baer

Pacific Northwest National Laboratory

304 PUBLICATIONS 5,564 CITATIONS

[SEE PROFILE](#)

# In Situ Mass Spectrometric Determination of Molecular Structural Evolution at the Solid Electrolyte Interphase in Lithium-Ion Batteries

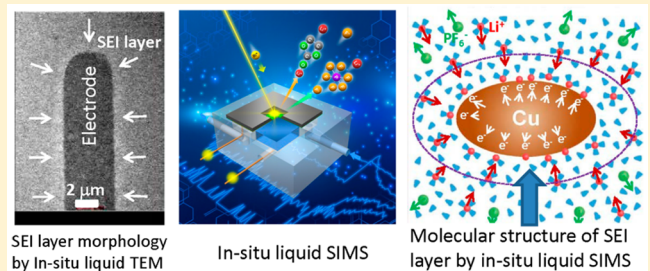
Zihua Zhu,<sup>\*,†</sup> Yufan Zhou,<sup>†,‡</sup> Pengfei Yan,<sup>†</sup> Rama Sesha Vemuri,<sup>†</sup> Wu Xu,<sup>§,||</sup> Rui Zhao,<sup>†</sup> Xuelin Wang,<sup>‡</sup> Suntharampillai Thevuthasan,<sup>†</sup> Donald R. Baer,<sup>†</sup> and Chong-Min Wang<sup>\*,†,||</sup>

<sup>†</sup>Environmental Molecular Sciences Laboratory, <sup>§</sup>Energy and Environmental Directorate, and <sup>||</sup>Joint Center for Energy Storage Research, Pacific Northwest National Laboratory, Richland, Washington 99352, United States

<sup>‡</sup>School of Physics, State Key Laboratory of Crystal Materials & Key Laboratory of Particle Physics and Particle Irradiation (MOE), Shandong University, Jinan 250100, China

## Supporting Information

**ABSTRACT:** Dynamic structural and chemical evolution at solid–liquid electrolyte interface is always a mystery for a rechargeable battery due to the challenge to directly probe a solid–liquid interface under reaction conditions. We describe the creation and usage of in situ liquid secondary ion mass spectroscopy (SIMS) for the first time to directly observe the molecular structural evolution at the solid–liquid electrolyte interface for a lithium (Li)-ion battery under dynamic operating conditions. We have discovered that the deposition of Li metal on copper electrode leads to the condensation of solvent molecules around the electrode. Chemically, this layer of solvent condensate tends to be depleted of the salt anions and with reduced concentration of Li<sup>+</sup> ions, essentially leading to the formation of a lean electrolyte layer adjacent to the electrode and therefore contributing to the overpotential of the cell. This observation provides unprecedented molecular level dynamic information on the initial formation of the solid electrolyte interphase (SEI) layer. The present work also ultimately opens new avenues for implanting the in situ liquid SIMS concept to probe the chemical reaction process that intimately involves solid–liquid interface, such as electrocatalysis, electrodeposition, biofuel conversion, biofilm, and biominerization.



**KEYWORDS:** *In situ liquid SIMS, solid–liquid interface, molecular structural evolution, lithium ion battery, SEI layers*

The operation of a lithium (Li)-ion battery relies on the reversible shuttling of conducting ions in the electrolyte between the two electrodes that are separated by the electrolyte.<sup>1–5</sup> The rechargeable capacity and the battery life depend critically on the structural stability of the electrodes themselves, the electrolyte degradation rate, and the electrode–electrolyte interaction layer—the so-called solid electrolyte interphase (SEI) layer.<sup>6</sup> Li<sup>+</sup> ions in the electrolyte are usually solvated. Upon entering the electrode, the solvated ions will be desolvated, leading to the accumulation of desolvation sheath components on or at the electrode. These accumulated components contribute to the formation of the SEI layers.<sup>7</sup> The formation of the SEI affects the Li<sup>+</sup> ion transport process and therefore the performance of the battery.<sup>8,9</sup> However, understanding of the SEI formation, structural and chemical nature of the SEI layer,<sup>10,11</sup> evolution of the SEI during the cyclic charge/discharge of the battery, and their correlation with Li<sup>+</sup> ion transport remains elusive and is therefore limited to the advancement of rechargeable Li-ion battery performance.<sup>12–15</sup>

Over the past few years tremendous progress has been made toward direct in situ observation of structural and chemical evolution of electrodes used for Li-ion batteries.<sup>16–21</sup> Recently, based on in situ liquid cell transmission electron microscopy

(TEM), it seems possible to directly observe the SEI layer formation and dendritic growth of Li metal-on-metal electrodes,<sup>22–24</sup> as representatively shown in Figure 1 and the in situ TEM movie in the Supporting Information (Movie S1). Fundamentally, the in situ TEM observations provide vivid morphological information on the evolution of electrode surface. However, the chemical composition and structure of the SEI cannot be directly captured by imaging through the liquid layers in the setup of the in situ TEM. Furthermore, questions about the specific species migrating within the liquid electrolyte and the ways they interact with the electrode cannot be readily answered by in situ TEM. To address these questions, we describe the creation of liquid-cell secondary ion mass spectrometry (SIMS) approach for in situ or more precisely operando SIMS studies of Li-ion batteries, gaining for the first time molecular level information that evolves at both the electrode surface and in the liquid electrolyte during the charge and discharge of the battery. We observed that, upon charging of the battery, the salt anions (hexafluorophosphate

**Received:** June 22, 2015

**Revised:** July 23, 2015

**Published:** August 19, 2015

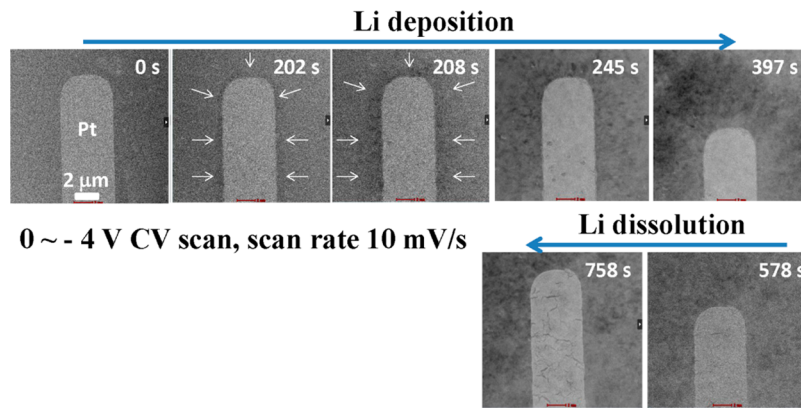


**Figure 1.** STEM high-angle annular dark field (HAADF) images of Li deposition and dissolution at the interface between the Pt working electrode and the  $\text{LiPF}_6/\text{PC}$  electrolyte during the charge/discharge cycles using in situ liquid cell TEM. The formation of the SEI layer is indicated by the arrows in the second frame. It is impossible to directly probe the SEI layer chemistry through the liquid.

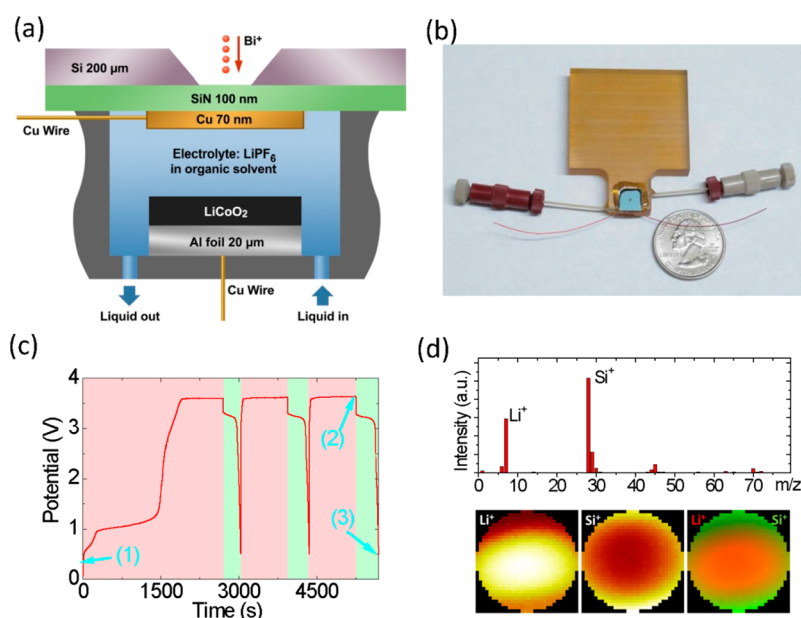


**Figure 2.** Fundamental concept on the setup of the in situ liquid SIMS for probing the electrode/electrolyte interface of a rechargeable Li-ion battery. (a) A schematic drawing of the liquid cell device with both anode and cathode integrated into the liquid cell. More details of the cell design can be found in Supporting Information. (b) A photo of the real device. (c) A typical galvanostatic charge and discharge curve of the cell. The charging regions are colored with pink, and the discharging regions are colored with green. SIMS data are collected at (1) fresh cell, (2) after the third charging, and (3) after the third discharging. A typical positive ion mass spectrum and two ion images ( $\text{Li}^+$  and  $\text{Si}^+$ ) are shown in d. During SIMS measurement, the cell is disconnected from power supply.

( $\text{PF}_6^-$ ) anions in this work) were repelled from the anode side,  $\text{Li}^+$  ions were reduced at the anode, leading to a liquid layer with a significantly low concentration of  $\text{Li}^+$  and  $\text{PF}_6^-$  around the anode. Formation of the lean electrolyte layer around the electrode will lead to reduced ionic conductivity and therefore contributing to the overpotential of the battery. The present work opens the door for in situ SIMS studies of both dynamic structural and chemical evolution of the electrodes and the SEI layer formation in batteries using real battery relevant electrolytes.

The basic concept for carrying out in situ liquid SIMS has been described in prior publications.<sup>25,26</sup> In essence, the liquid to be analyzed is exposed by creating a small hole into which a probing primary beam can interact with the liquid. In order to make this concept for in situ observation of electrode reactions in a rechargeable battery, a new cell was designed and fabricated using Ultem block. An electrode created by coating  $\text{LiCoO}_2$

powder particles on Al foil was used as cathode. The anode side was fabricated on a silicon chip with a “transparent”  $\text{Si}_3\text{N}_4$  membrane window of 100 nm in thickness and lateral dimensions of 0.5 mm × 0.5 mm. A Cu film of ~70 nm was sputter deposited on the  $\text{Si}_3\text{N}_4$  film/window. The Cu film had a granular structure as shown by the SEM image in the Supporting Information (Figure S1). An electrolyte comprised of 1.0 M  $\text{LiPF}_6$  in 1:2 (v/v) ethylene carbonate:dimethyl carbonate ( $\text{LiPF}_6$  in EC:DMC) was used. A cross-section of the electrochemical cell is illustrated in Figure 2a. Following the assembling of the cell, the liquid electrolyte was filled in an argon glovebox and sealed at the end of the fill-tube as illustrated in Figure 2b. Electrochemical characteristics of the cell were evaluated by galvanostatic charge and discharge process (Figure 2c). The overall structure of the liquid cell is illustrated by the animation that can be found in the Supporting Information (Movie S2).

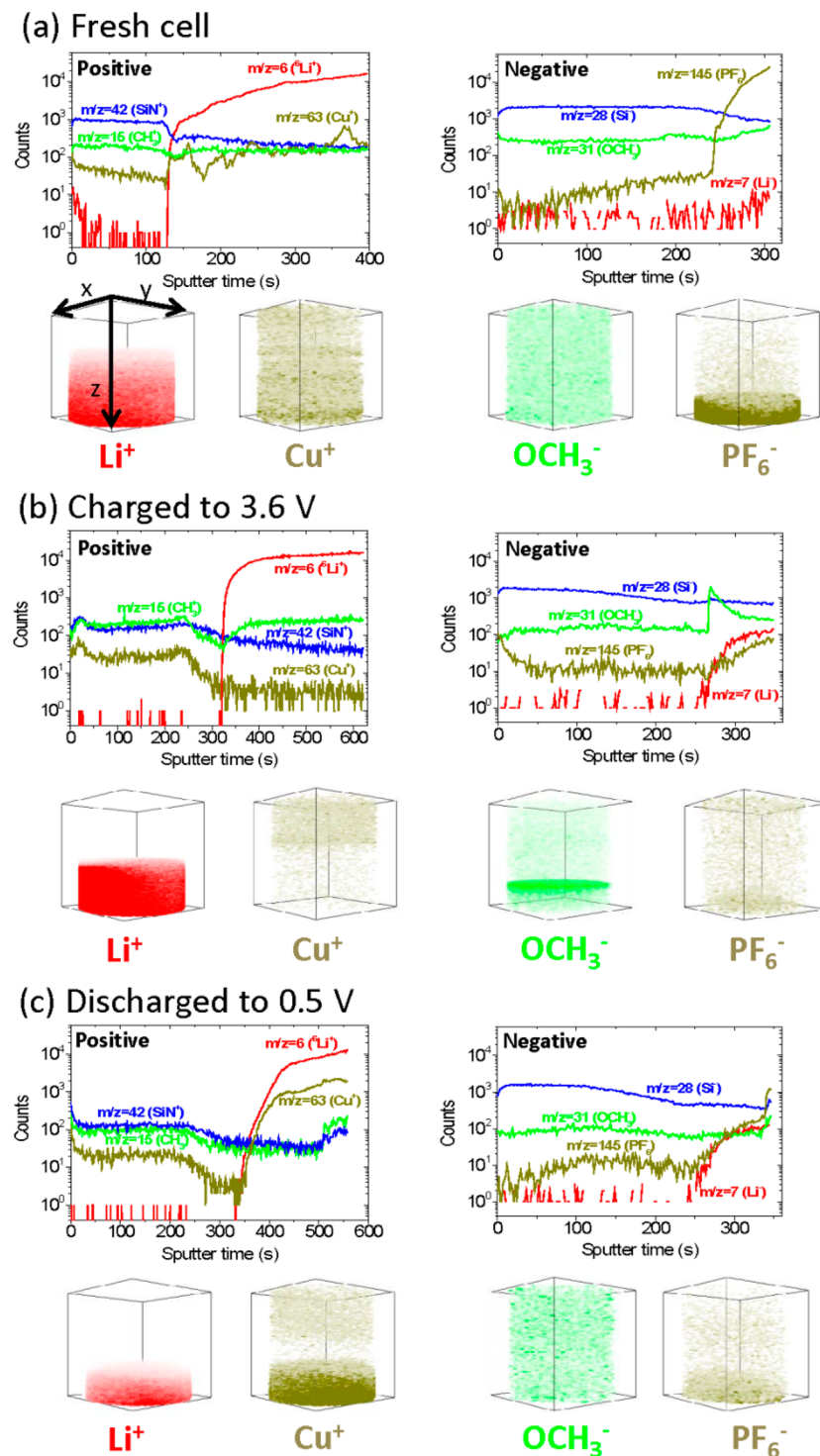


**Figure 3.** ToF-SIMS depth profiling and the constructed 3D configuration of several representative positive and negative secondary ions at the vicinity of the anode surface before and after charging/discharging of the battery. (a) Fresh cell, (b) charged to 3.6 V, and (c) discharged to 0.5 V. The data are collected at the (1), (2), and (3) locations as shown in the Figure 2c.

The electrode/electrolyte interface was *in situ* analyzed using SIMS when the cell was freshly assembled, charged, and discharged. Data were collected, while the primary ion beam created a small hole in the  $\text{Si}_3\text{N}_4$  window, into the Cu film and the electrolyte. The SIMS analysis was carried out using a TOF-SIMS5 instrument (IONTOF GmbH, Germany). A pulsed 25 keV  $\text{Bi}^+$  beam was focused to a diameter of  $\sim 450$  nm (tuned on a reference Cu grid). The pulse frequency was  $\sim 25$  kHz, and

the beam current was  $\sim 3.0$  pA. During measurements the  $\text{Bi}^+$  beam was scanned on a round area of a diameter of  $\sim 2 \mu\text{m}$  on the  $\text{Si}_3\text{N}_4$  window. A mass spectrum, depth profiles, and 2-demensional ion images were simultaneously collected. In addition, 3-dimensional ion images can be reconstructed as shown in the Supporting Information (Figure S2). During SIMS measurements, the pressure in the analysis chamber was about  $1\text{--}2 \times 10^{-6}$  mbar. Normally, several ( $\geq 5$ ) holes could be

punched on a  $\text{Si}_3\text{N}_4$  window during one set of experiment, so multimeasurements (e.g., before and after charging/discharging) on the same cell is feasible. However, some  $\text{Si}_3\text{N}_4$  windows might be broken after only 2–3 measurements.

The liquid to be analyzed is exposed by creating a small hole into which a probing primary beam can interact with the liquid as shown in **Figure 2** and the Figures in the **Supporting Information** (Figure S2). The depth profiles of eight representative secondary ions (four positive ions and four negative ions) before charge and discharge cycle of the battery are shown in **Figure 3a**. Molecular information captured at this stage (the fresh battery cell) essentially reflects structural modifications of the electrode surface as a consequence of the static interaction between the electrolyte and the electrode. Due to the porous granular structure of the deposited copper (Cu) film,  $\text{Li}^+$  and  $\text{PF}_6^-$  signals were detected immediately following the  $\text{Si}_3\text{N}_4$  film was sputtered through, indicating that the electrolyte with the ionized species can permeate to the  $\text{Si}_3\text{N}_4/\text{Cu}$  interface. In addition,  $\text{Cu}^+$  signals can be observed after sputtering through the  $\text{Si}_3\text{N}_4$  film. However, we noticed that although the  $\text{Si}_3\text{N}_4/\text{Cu}$  interface can be exposed and readily identified, it is very hard to sputter through the Cu layer even for more than 800 s sputtering. In contrast, for a control experiment of sputtering of a 70 nm thick Cu film on a  $\text{Si}_3\text{N}_4$  film (without electrolyte), it took only ~40 s to penetrate the Cu film. A plausible explanation for the observation of the significantly slow sputtering of the Cu film with the liquid electrolyte is that, after the  $\text{Si}_3\text{N}_4$  film was penetrated, the electrolyte was able to continuously diffuse through the porous Cu film, impeding sputtering of the Cu film. As demonstrated in a later stage, the use of porous Cu film actually offers the advantage of allowing the detection of electrode surface reactions.

Identification of ion species and understanding the depth profiles from the solvent species at this initial stage is of interest as it provides the baseline for comparing the species observed after charge and discharge of the battery. Significant identifiable ion species include  $\text{H}^+$ ,  $\text{C}^+$ ,  $\text{CH}^+$ ,  $\text{CH}_2^+$ ,  $\text{CH}_3^+$ ,  $\text{OCH}_3^+$ ,  $\text{H}^-$ ,  $\text{C}^-$ ,  $\text{CH}^-$ ,  $\text{C}_2^-$ ,  $\text{C}_2\text{H}^-$ , and  $\text{OCH}_3^-$ , with many other minor peaks. For the reader's convenience, the  $\text{CH}_3^+$  and  $\text{OCH}_3^-$  are used as two representative ions in **Figure 3**. These species show a significant background in the  $\text{Si}_3\text{N}_4$  film and a mild and slow increase after sputtering through the  $\text{Si}_3\text{N}_4$  film, which is quite different from the jumping up behavior of the  $\text{Li}^+$  and  $\text{PF}_6^-$  signals. The high background of these signals may attribute to the relatively high pressure ( $\sim 1.5 \times 10^{-6}$  mbar) of residual gases in the analysis chamber. It is reasonable to expect more of a jump behavior when the  $\text{Si}_3\text{N}_4$  is penetrated for these solvent-related ion species if the pressure in the analysis chamber can be significantly reduced (e.g.,  $< 1 \times 10^{-8}$  mbar).

Upon charging the battery to 3.6 V, the depth profiles of the eight representative secondary ions are shown in **Figure 3b** (the galvanostatic charge curve is shown as **Figure 2c**). As compared with the fresh cell, four features were typically observed for the charged sample. (1) Following the charging, the  $\text{Li}^+$  signal shows a steeper increase upon sputtering through of the  $\text{Si}_3\text{N}_4$  film, likely indicating the deposition of Li metal on the Cu electrode surface, which is morphologically very well illustrated by the recent in situ TEM observations and representatively shown in **Figure 1**.<sup>22–24</sup> Consistent with the argument of the deposition of Li metal on the Cu electrode is the observation of a decrease of the  $\text{Cu}^+$  signal when compared to the data before charging. (2) There is a dramatic relative decrease of the  $\text{PF}_6^-$

signal as compared with the case of the fresh sample, indicating that during the charging of the battery  $\text{PF}_6^-$  ions migrate toward the cathode direction and leading to the significantly decreased concentration of  $\text{PF}_6^-$  at the vicinity of the anode. (3) Interestingly, following the charging, the solvent signals from negative ion depth profiles (e.g.,  $\text{H}^-$ ,  $\text{C}^-$ ,  $\text{CH}^-$ ,  $\text{C}_2^-$ ,  $\text{C}_2\text{H}^-$ ,  $\text{OCH}_3^-$ ; with  $\text{OCH}_3^-$  used as a representative in **Figure 3b**) show an immediate jump after sputtering through the  $\text{Si}_3\text{N}_4$  film and gradually decrease with time with the balance signal intensity being still higher than that in the  $\text{Si}_3\text{N}_4$  film. The  $\text{Li}^-$  signal can be detected, and it does not show an immediate jump as soon as the sputtering through of the  $\text{Si}_3\text{N}_4$  film occurs. (4) Based on charge calculation, it is estimated that for each charging the Li deposited on the Cu electrode is ~50 nm in thickness. However, it is very difficult to sputter through the Li layer to reach the Cu layer even after long-time sputtering (as shown in **Figure S3e**). These observations are all consistent with the formation of a solvent-enriched layer between the  $\text{Si}_3\text{N}_4$  film and the Li/Cu electrode. This point is further consistently supported by the observation following the discharging of the battery as described in the subsequent section.

After discharging the battery, the SIMS depth profiles are shown in **Figure 3c**. As compared with the case of the charged state of the battery, following the discharging, the  $\text{Li}^+$  signal only decreases slightly, and correspondingly, the  $\text{PF}_6^-$  signal only shows a moderate increase. These observations clearly indicate that, upon the discharging of the battery, the deposited Li metal layer is not fully reversibly stripped off, suggesting formation of a dead Li layer. At the same time, the  $\text{PF}_6^-$  anions are not totally recovered to the case of before charging. These observations is consistent with the direct in situ TEM observation of the nonreversible stripping of Li metal from the Cu electrode upon discharging.<sup>22,23</sup> The formation of nonreversible Li species is also supported by the behaviors of the Cu signals. Following the discharging, the  $\text{Cu}^+$  signal increases dramatically. At the same time, the Cu layer can be sputtered through as demonstrated by a dramatic increase of solvent-related signals at the end stage of depth profiles (as shown in **Figure 3c**,  $> 510$  s for positive secondary ion depth profiles, or  $> 335$  s for negative secondary ion depth profiles). Collectively these observations can be explained by the postulation that, after discharging, most of the channels in the porous Cu film are filled or covered by the dead Li species, blocking or inhibiting the liquid to reach the  $\text{Si}_3\text{N}_4/\text{electrode}$  interface. This explanation is supported by the cyclic galvanostatic charge/discharge curves shown in **Figure 2c** and **Figure S4**, where the charging time is much longer than the discharging time for each charging/discharging cycle. Since a constant current was used during the charge/discharge, a shorter discharging time than that of charging indicates either certain fraction of  $\text{Li}^+$  reacts with solvent to form insoluble Li salts or the covering up of the formed Li metal by the insoluble Li salts. The nonreversible Li species is essentially part of the SEI layer, which is apparently thickening with each cyclic progression of charging and discharging the battery, contributing to depletion of active Li in the battery system and therefore leading to the capacity fading and eventual failure of the battery.

As shown in **Figure S4**, the model battery can be charged and discharged at least 10 cycles. The SIMS profiles show a reasonably good repeatability before and after several charging/discharging cycles as shown in **Figure S3**. The good repeatability of our data provides consistent evidence to

support above description. For example, the  $\text{CH}_3^+$  signal (after punching through, coming from solvent) intensity after discharging decreases to 30–40% of that before discharging. However, after recharging, the  $\text{CH}_3^+$  signal intensity can be recovered. Also, the  $\text{CH}_3^+$  signal after charging is comparable with that of the fresh cell. These observations suggest that more solvent molecules can be detected after charging than after discharging, supporting that a solvent-enriched layer exists at the  $\text{Si}_3\text{N}_4$ /electrode interface after charging. In addition, in negative ion profiles, the immediate jump of the solvent signals at the  $\text{Si}_3\text{N}_4$ /electrode interface was not observed in the fresh cell or after discharging, indicating that a normal electrolyte (solvent with  $\text{Li}^+$  and  $\text{PF}_6^-$ ) layer cannot provide an immediate jump of negative ions of the solvent as soon as the  $\text{Si}_3\text{N}_4$  film was sputtered through.

For Li-ion batteries or more broadly other rechargeable batteries, three critical questions need to be answered: (1) How do the cation and anion from the salt interact with the solvent molecules? (2) How does such an interaction affect the mobility of the ions? and (3) What is the consequence of the electrode surface structural modification by the repeated ion insertion and extraction? Great research efforts of both theoretical and experimental nature have been made intending to answer these questions. The present *in situ* SIMS observation of the formation of the solvent condensate layer and nonreversible Li species above the Li layer is significant. Dissolution of salt in a solvent has been well-understood, described as the dispersion of cations and anions of the salt in the solvent. Under an electrical field, the oppositely charged ions move toward opposite directions of attracting charge. This classic model of salt–solvent system is definitely true for the case of the electrolyte system in a rechargeable battery, as clearly demonstrated by the present *in situ* liquid SIMS observation. Upon charging, the instantaneous formation of the solvent condensate layer on the electrode surface leads to the localized liquid layer of depletion of  $\text{PF}_6^-$  and with a low concentration of  $\text{Li}^+$ , which is essentially a layer with decreased ionic conductance, therefore contributing to the overpotential of the battery cell.

The study of solvation–desolvation of active ions in electrolytes has been mostly relied on electrospray ionization (ESI)<sup>15</sup> and nuclear magnetic resonance (NMR) coupled with theoretical calculations,<sup>14</sup> which are mostly bulk analysis techniques and hard to be used for studying the solvation–desolvation process occurring at the electrode/electrolyte interface. In contrast, the *in situ* liquid SIMS approach described here can readily provide relevant information at the solid/liquid interface. In addition, it should be noted that our *in situ* liquid SIMS data suggest that  $\text{Li}^+$  prefers to form solvation layer with ethylene carbonate (EC) than dimethyl carbonate (DMC) in the 1:2 EC–DMC solution as shown in Figure S5. This observation is consistent with previously reported results based on *ex situ* methods.<sup>14</sup> It has been generally established that the solvation sheath for  $\text{Li}^+$  ions shows a preference of one type of solvent over the other for the case of mixed solvents, such as cyclic over acyclic carbonate.<sup>15</sup> The solvation sheath structure of  $\text{Li}^+$  depends on the ratios of cyclic such as EC to linear carbonates such as DMC.<sup>12</sup>  $\text{Li}^+$  will preferentially bind to the polar molecules in a mixture of solvents, such as EC may become a major component for the  $\text{Li}^+$  sheath.<sup>14</sup> A generally perceived pictorial description therefore would be the cation, such as  $\text{Li}^+$  for the case of Li-ion battery, is solvated; the motion of the cation will carry with the solvation sheath; and before the

ion gets into to the electrode, desolvation contributes to the formation of the SEI layer. Apparently, the  $\text{Li}^+$  solvation sheath structure is a critical component for defining the local structure and chemistry at the very vicinity of the electrode, because the solvation molecules are left behind by the  $\text{Li}^+$  before  $\text{Li}^+$  gets into the electrode.

The structure and formation mechanism of SEI has been extensively investigated using various sophisticated techniques.<sup>7,11,27–29</sup> For example, based on *ex-situ* X-ray photoelectron spectroscopy (XPS), Raman, and infrared (IR) studies, it has been found that the SEI layer formation on hydrogenated amorphous Si (a-Si:H) anodes is featured by the decomposition of the  $\text{LiPF}_6$ -based electrolyte to  $\text{LiF}$ ,  $\text{Li}_x\text{PF}_y$ , and  $\text{PF}_5$  at a voltage of 1.8 V.<sup>27</sup> It has been reported that, while inorganic components of the SEI may be more electrochemically stable than the organic phase, they may also significantly decrease  $\text{Li}^+$  transport.<sup>9,28</sup> One of the key shortcomings of these observations of SEI layers, in addition to the nature of *ex situ* rather than *in situ*, is the lack of molecular information that is spatially adjacent to the electrolyte/electrode interface. Direct molecular level observation of structural and chemical evolution of electrode surface in a rechargeable battery has not previously been possible. The present *in situ* SIMS analysis of molecular species evolution at the electrode during the charging and discharging of the battery provides unprecedented information regarding the structure of the electrolyte and the migrating species. The *in situ* SIMS observation results described above provide a clearer view of electrode reaction for Li-ion battery than previously possible, which is schematically illustrated in Figure 4. Upon charging the battery, Li metal is deposited on the anode and part of which is a dead Li deposition, while  $\text{PF}_6^-$  ions migrate toward the cathode, leading to a solvent-enriched liquid layer formation that is adjacent to the Li metal. This layer of liquid is depletion of  $\text{PF}_6^-$  and with a low concentration of  $\text{Li}^+$ . Upon discharging, the reversible fraction of Li metal is stripped off. Based on the *in situ* TEM observation, Holtz et al. have noticed that, upon discharging, the electrolyte adjacent to the  $\text{LiFePO}_4$  cathode can be instantaneously depleted of  $\text{Li}^+$  ions,<sup>21</sup> which is consistent with what has been observed here on the formation of solvent condensate layer at the anode. On a broad basis, the present work opens a new avenue to use the SIMS to probe solid/liquid interface on a molecular level.

**Conclusions.** The classic physics and chemistry tell us that, under an electrical field, charged ions with opposites signs move toward opposite directions as for the case of a rechargeable battery during charge and discharge processes. The fundamental challenge is what is the structural nature of the charged ions in the liquid and the consequences of the ions insertion into the electrode. Using *in situ* liquid SIMS, we directly observed the molecular information on rechargeable Li-ion battery under battery operating conditions. We discovered that, upon charging, the solvated  $\text{Li}^+$  ions migrate to the negative electrode (i.e., anode), and the negatively charged  $\text{PF}_6^-$  ions drift toward the positive electrode (i.e., cathode) side. Following the deposition of Li, a thin layer of solvent was formed at the anode side, which shows the tendency of instantaneous depletion of  $\text{PF}_6^-$  and with a low concentration of  $\text{Li}^+$ . With charge and discharge cycling, insoluble Li salts gradually form and accumulate on the Cu electrode surface. The *in situ* liquid SIMS direct observation of molecular information on electrode surface will greatly impact the research work of electrochemical community, especially dealing

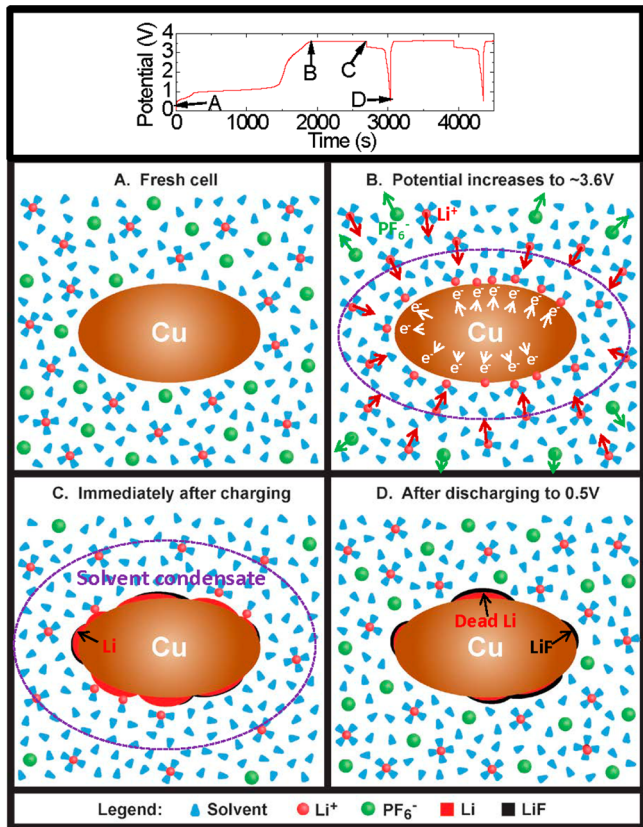


**Figure 4.** A schematic illustration showing the molecular level stripping and clustering during the charge–discharge of a Li-ion battery. The top panel shows the charge–discharge curves and the corresponding molecular migration is illustrated in A through D. (A) At the fresh cell state,  $\text{PF}_6^-$  and solvated  $\text{Li}^+$  ions are evenly distributed in the electrolyte. (B) When a potential is applied on the anode Cu nanoparticles, the  $\text{PF}_6^-$  ions are repelled from the electrolyte around the Cu nanoparticles. When the potential increases to around 3.6 V, solvated  $\text{Li}^+$  ions start to lose solvent molecules and are reduced to metallic Li. (C) Immediately after charging, a layer of metallic Li forms on the Cu surface, while a solvent layer with a low concentration of  $\text{Li}^+$  and depletion of  $\text{PF}_6^-$  forms around the Cu nanoparticle. (D) After discharging, partial of metallic Li was stripped back into electrolyte; however, some cannot be stripped because of the formation of an inert Li salt layer on top of the metallic Li.

with liquid/solid interfaces under dynamic operating conditions.

## ■ ASSOCIATED CONTENT

### S Supporting Information

The Supporting Information is available free of charge on the ACS Publications website at DOI: [10.1021/acs.nanolett.5b02479](https://doi.org/10.1021/acs.nanolett.5b02479).

Additional information regarding the details the in situ SIMS device, additional results ([PDF](#))

In situ TEM movie ([AVI](#))

Animation of the overall structure of the liquid cell ([AVI](#))

## ■ AUTHOR INFORMATION

### Corresponding Authors

\*E-mail: [Zihua.Zhu@pnnl.gov](mailto:Zihua.Zhu@pnnl.gov).

\*E-mail: [Chongmin.Wang@pnnl.gov](mailto:Chongmin.Wang@pnnl.gov).

## Notes

The authors declare no competing financial interest.

## ■ ACKNOWLEDGMENTS

The authors appreciate the beneficial discussion with Dr. Kang Xu of Army Research Laboratory. This work was supported by Joint Center for Energy Storage Research (JCESR), an Energy Innovation Hub funded by the Department of Energy, Office of Science, Basic Energy Sciences. The development of the in situ and operando SIMS concept and device were supported by the Chemical Imaging Initiative, a Laboratory Directed Research and Development Program at Pacific Northwest National Laboratory (PNNL). The fabrication of the in situ TEM and in situ SIMS cell was supported by the Assistant Secretary for Energy Efficiency and Renewable Energy, Office of Vehicle Technologies of the U.S. Department of Energy under Contract No. DE-AC02-05CH11231, Subcontract No. 6951379 under the advanced Battery Materials Research (BMR) program. PNNL is a multiprogram national laboratory operated by Battelle for the U.S. Department of Energy (DOE) under Contract DE-AC05-76RL01830. The research was performed using the Environmental Molecular Sciences Laboratory (EMSL), a national scientific user facility sponsored by the Department of Energy's Office of Biological and Environmental Research and located at PNNL.

## ■ REFERENCES

- (1) Armand, M.; Tarascon, J.-M. *Nature* **2008**, *451*, 652–657.
- (2) Tarascon, J. M.; Armand, M. *Nature* **2001**, *414* (6861), 359–367.
- (3) Poizot, P.; Laruelle, S.; Gruegeon, S.; Dupont, L.; Tarascon, J. M. *Nature* **2000**, *407* (6803), 496–499.
- (4) Kang, B.; Ceder, G. *Nature* **2009**, *458* (7235), 190–193.
- (5) Scrosati, B. *Nature* **1995**, *373* (6515), 557–558.
- (6) Aurbach, D.; Zinigrad, E.; Cohen, Y.; Teller, H. *Solid State Ionics* **2002**, *148*, 405–416.
- (7) Verma, P.; Maire, P.; Novák, P. *Electrochim. Acta* **2010**, *55*, 6332–6341.
- (8) Aurbach, D. *J. Power Sources* **2000**, *89*, 206–218.
- (9) Peled, E.; Golodnitsky, D. *Lithium-ion Batteries: Solid-electrolyte Interphase*; Imperial College: London, 2004.
- (10) Ding, F.; Xu, W.; Graff, G. L.; Zhang, J.; Sushko, M. L.; Chen, X.; Shao, Y.; Engelhard, M. H.; Nie, Z.; Xiao, J.; Xingjiang, L.; Sushko, P. V.; Liu, J.; Zhang, J.-G. *J. Am. Chem. Soc.* **2013**, *135*, 4450–4456.
- (11) Cresce, A. v.; Russell, S. M.; Baker, D. R.; Gaskell, K. J.; Xu, K. *Nano Lett.* **2014**, *14*, 1405–1412.
- (12) Xu, K. *J. Electrochem. Soc.* **2007**, *154* (3), A162–A167.
- (13) Xu, K.; Cresce, A. v.; Lee, U. *Langmuir* **2010**, *26* (13), 11538–11543.
- (14) Xu, K.; Lam, Y.; Zhang, S. S.; Jow, T. R.; Curtis, T. B. *J. Phys. Chem. C* **2007**, *111*, 7411–7421.
- (15) von Cresce, A. v.; Xu, K. *Electrochim. Solid-State Lett.* **2011**, *14*, A154–A156.
- (16) Wang, C. M.; Xu, W.; Liu, J.; Choi, D. W.; Arey, B.; Saraf, L. V.; Zhang, J. G.; Yang, Z. G.; Thevuthasan, S.; Baer, D. R.; Salmon, N. J. *Mater. Res.* **2010**, *25*, 1541–1547.
- (17) Huang, J. Y.; Zhong, L.; Wang, C. M.; Sullivan, J. P.; Xu, W.; Zhang, L. Q.; Mao, S. X.; Hudak, N. S.; Liu, X. H.; Subramanian, A.; Fan, H.; Qi, L.; Fukushima, A.; Li, J. *Science* **2010**, *330* (6010), 1515–1520.
- (18) Gu, M.; Parent, L. R.; Mehdi, B. L.; Unocic, R. R.; McDowell, M. T.; Sacci, R. L.; Xu, W.; Connell, J. G.; Xu, P.; Abellán, P.; Chen, X.; Zhang, Y.; Pereira, D. E.; Evans, J. E.; Lauhon, L. J.; Zhang, J.-G.; Liu, J.; Browning, N. D.; Cui, Y.; Arslan, I.; Wang, C.-M. *Nano Lett.* **2013**, *13* (12), 6106–6112.
- (19) Sacci, R. L.; Dudney, N. J.; More, K. L.; Parent, L. R.; Arslan, I.; Browning, N. D.; Unocic, R. R. *Chem. Commun.* **2014**, *50*, 2104–2107.

- (20) Zeng, Z.; Liang, W.-I.; Liao, H.-G.; Xin, H. L.; Chu, Y.-H.; Zheng, H. *Nano Lett.* **2014**, *14*, 1745–1750.
- (21) Holtz, M. E.; Yu, Y.; Gunceler, D.; Gao, J.; Sundararaman, R.; Schwarz, K. A.; Arias, T. S. A.; Abruña, H. C. D.; Muller, D. A. *Nano Lett.* **2014**, *14*, 1453–1459.
- (22) Sacci, R. L.; Black, J.; Balke, N.; Dudney, N. J.; More, K. L.; Unocic, R. R. *Nano Lett.* **2015**, *15*, 2011–2018.
- (23) Mehdi, B. L.; Qian, J.; Nasybulin, E.; Park, C.; Welch, D. A.; Faller, R.; Mehta, H.; Henderson, W. A.; Xu, W.; Wang, C. M.; Evans, J. E.; Liu, J.; Zhang, J.-G.; Mueller, K. T.; Browning, N. D. *Nano Lett.* **2015**, *15*, 2168–2173.
- (24) Leenheer, A. J.; Jungjohann, K. L.; Zavadil, K. R.; Sullivan, J. P.; Harris, C. T. *ACS Nano* **2015**, *9*, 4379–4389.
- (25) Yang, L.; Yu, X.-Y.; Zhu, Z.; Iedema, M. J.; Cowin, J. P. *Lab Chip* **2011**, *11*, 2481–2484.
- (26) Liu, B.; Yu, X.-Y.; Zhu, Z.; Hua, X.; Yang, L.; Wang, Z. *Lab Chip* **2014**, *14*, 855–859.
- (27) Arreaga-Salas, D. E.; Sra, A. K.; Roodenko, K.; Chabal, Y. J.; Hinkle, C. L. *J. Phys. Chem. C* **2012**, *116*, 9072–9077.
- (28) Schroder, K. W.; Celio, H.; Webb, L. J.; Stevenson, K. J. *J. Phys. Chem. C* **2012**, *116*, 19737–19747.
- (29) McArthur, M. A.; Trussler, S.; Dahn, J. R. *J. Electrochem. Soc.* **2012**, *159*, A198–A207.